Designing Ceria/Alumina for Efficient Trapping of Platinum Single Atoms

Hien N. Pham[1], Andrew DeLaRiva[1], Eric J. Peterson[1], Ryan Alcala[1], Konstantin Khivantsev[2], János Szanyi[2], Xiaohong S. Li[2], Dong Jiang[3], Weixin Huang[3], Yipeng Sun[4], Pascaline Tran[4], Quan Do[5], Craig L. DiMaggio[5], Yong Wang[2,3,*] and Abhaya K. Datye[1,*]

1. Department of Chemical and Biological Engineering, and Center for Microengineered Materials, University of New Mexico, Albuquerque, NM 87131, USA
2. Institute for Integrated Catalysis, Pacific Northwest National Laboratory, Richland, WA 99352, USA
3. The Gene and Linda Voiland School of Chemical Engineering and Bioengineering, Washington State University, Pullman, WA 99164, USA
4. BASF Corporation, Iselin, NJ 08830, USA
5. Stellantis N.V., Auburn Hills, MI 48326, USA

Corresponding authors: datye@unm,edu
wang42@wsu.edu

KEYWORDS: Single atoms, Ceria-alumina, Stability, PGM catalysts, Trapping efficiency, CO oxidation

Abstract

Cerium oxide (ceria) has been shown to be very effective at trapping platinum atoms, due to formation of stable surface complexes at step edges, where coordinatively unsaturated cerium cations are present. But ceria loses its effectiveness when heated to high temperatures, due to loss of surface area and growth in particle size associated with sintering of the oxide. Being a rare-earth, and with limited supplies worldwide, it is important to develop methods to improve the effectiveness of ceria as a catalyst support. Here we explore the performance for trapping Pt atoms when the ceria is supported on a high surface area alumina carrier. This helps create a more sustainable catalyst formulation, especially if we can retain the high dispersion of Pt seen on ceria supports. For this work, we studied the atom trapping efficacy of ceria/alumina samples with increasing ceria content (8 wt% - 50%) and contrasted the behavior with pure ceria. Electron microscopy reveals that when dispersed on alumina, ceria is present in the form of crystalline nanoparticles as well as isolated cerium ions. These two forms of ceria differ markedly in their ability to trap Pt atoms. Atomically dispersed cerium is present in the form of Ce^{3+} cations on alumina, however this form of ceria is not effective for trapping Pt atoms. Our results show that the atom trapped Pt resides primarily on crystalline ceria nanoparticles. CO oxidation was used as a probe reaction to evaluate the performance of these Pt_{AT}/ceria-alumina catalysts. We conclude that over the range of ceria loadings we investigated, 50% ceria/alumina represents the optimal catalyst support for achieving high surface area and atom trapping efficiency while helping reduce the total ceria content in this catalyst system.

Introduction

Transportation is a basic human need and access to transportation is associated with improved quality of life. All vehicles powered by hydrocarbon fossil fuels emit the greenhouse gas CO_2 and

toxic components such as CO, NO_x, particulate matter and unburnt hydrocarbons. The emissions can cause health issues, especially in crowded urban environments. Hence, treatment of the exhaust with catalytic emission control systems plays a major role in achieving the UN sustainable development goals for climate change and the environment [1]. To decrease greenhouse gas emissions, there is a push towards increased efficiency of engines. More efficient engines waste less heat in the tailpipe, as also do hybrid drive trains, so the exhaust is cooler. Furthermore, air pollutants such as CO, NO_x and hydrocarbons (HC) from the exhaust of vehicles, arise mainly during the cold-start process, since the current generation of catalysts are very effective once the catalyst warms up [2, 3]. Emission control catalysts therefore need to be effective at lower temperatures [2]. At the same time, these catalysts must withstand demanding driving conditions and last the lifetime of the car or truck. To achieve these goals, catalysts need to survive stringent protocols developed for accelerated aging [3]. To meet the criteria for future emission regulations, the catalysts should achieve at least 90% conversion of criteria pollutants by 150 °C (the US DOE 150 °C challenge) and maintain thermal/hydrothermal durability under harsh conditions encountered in automotive engine exhaust [2-4]. To achieve this performance, manufacturers add higher loading of the precious metals. Combined with a growth in the number of cars and trucks, automotive PGM demand continues to rise, with Pt, Pd and Rh prices increasing steadily. To make transportation more affordable and sustainable and to provide clean air worldwide, there is an urgent need to reduce the consumption of PGMs and rare earths in emission control systems. This is the focus of our study, aimed at lowering the need for Pt and the rare-earth cerium oxide in exhaust control devices.

Diesel oxidation catalysts (DOCs) are used for the oxidation of CO, HC, and NO under lean conditions. DOCs typically consist of Pt with added Pd to enhance stability. For efficient utilization of PGMs such as Pt, it is important to maximize the fraction of atoms at the surface, which is why PGMs are present in the form of nanoparticles on an oxide support. The efficacy of a nanoparticle is expressed in terms of the fraction of surface atoms (dispersion), and it varies inversely with particle diameter, with 100% dispersion being achieved when the PGMs are present as isolated single atoms. In industrial practice, especially with applications involving reactions at high temperatures, such as exhaust emission control, atoms become mobile and agglomerate to form large particles, losing efficiency [5]. To keep these atoms stable, they must be trapped on the catalyst support. Our previous work has shown that Pt can be trapped in the form of single atoms on ceria simply by heating the catalyst at 800 °C in flowing air [6]. Up to 3 wt% Pt could remain atomically dispersed on ceria, but when we exceeded the saturation capacity of ceria, we detected large metallic Pt particles [7]. The upper limit for stabilizing single atoms of Pt on ceria in our previous work was dictated by the thermal stability of ceria. It is known that ceria is not thermally stable and loses surface area during high temperature hydrothermal aging [8]. Recent reports show improved performance when ceria is supported on alumina [9, 10]. However, the effectiveness of ceria supported on alumina for atom trapping of Pt has not been investigated. Therefore, in this work, we have studied the efficacy of ceria for trapping Pt atoms when 1 wt% of Pt was supported on alumina with ceria loading varying from 8 wt% - 50 wt%. CO oxidation reactivity, CO-DRIFTS, XRD and AC-STEM were used to quantify the amount of Pt that could be trapped in the form of single atoms. As we show here, the 50% ceria/alumina has enough ceria sites to capture almost all the Pt, yielding higher reactivity than Pt deposited on polyhedral ceria (100% ceria).

Experimental Section

Catalyst Preparation

Three ceria/alumina samples, which represent commercially available samples from our industry co-authors, were used as supports for this study. We selected these ceria/alumina supports since initial results showed they were thermally stable at temperatures up to 1000 °C. The catalyst supports were 8 wt% CeO_2/92 wt % Al_2O_3 (CA08), 30 wt% CeO_2/70 wt % Al_2O_3 (CA30) and 50 wt% CeO_2/50 wt % Al_2O_3 (CA50). To establish that conventional impregnation and calcination would yield very similar samples, we prepared a 13 wt% ceria sample in our laboratory. The sample CA13 containing 13 wt% CeO_2/87 wt% Al_2O_3 (CA13) was prepared by incipient wetness impregnation using cerium (III) nitrate hexahydrate (Sigma Aldrich) on alumina (SASOL; SBA-150) followed by calcination at 800 °C for 6 hr in flowing air. 1 wt% Pt on ceria/alumina supports were prepared by incipient wetness impregnation using tetraammineplatinum (II) nitrate (Sigma Aldrich). After drying at 100 – 120 °C, the samples were calcined at 350 °C for 4 hr in air (box furnace) with 5 °C/min ramp rate. The samples were also calcined at 800 °C for 10 hr in air (box furnace) with 10 °C/min ramp rate, which causes the Pt to form single atoms via atom trapping (AT) [6]. For comparison, we used a laboratory-prepared ceria sample, which we have termed polyhedral ceria (PHC) in our previous work [8]. Polyhedral ceria (PHC) was prepared via the decomposition of cerium (III) nitrate hexahydrate. The nitrate was placed into a crucible and decomposed in a box furnace at 350 °C (1 °C/min ramp rate) for 4 hr. The resulting solid was then ground to a powder and used as the support to prepare 1 wt% Pt/PHC via the atom trapping approach used for the ceria/alumina samples.

Catalyst Characterization

Samples were dispersed in ethanol and mounted on holey carbon grids for examination in a JEOL NEOARM 200CF transmission electron microscope equipped with spherical aberration correction to allow atomic resolution imaging, and an Oxford Aztec Energy Dispersive System (EDS) for elemental analysis. The microscope is equipped with two large area JEOL EDS detectors for higher throughput in acquisition of x-ray fluorescence signals. Images were recorded in annular dark field (ADF) mode and in annular bright field (ABF) mode. ICP-AES was done at Galbraith Laboratories, Inc. with selected samples, to obtain elemental analysis. Powder X-ray diffraction (XRD) was performed using a Rigaku SmartLab diffractometer equipped with a Cu-target X-ray source (40 kV, 40 mA), a D/teX Ultra 1-D position sensitive detector, and a Ni-foil filter for reduction of the Cu-Kβ component of the diffracted radiation. Data was collected from 20 – 150° 2θ with a step size of 0.02°, and the crystallite sizes, composition and lattice constants were obtained using the MDI Jade software. BET surface area and pore structure analysis was performed via N_2 adsorption at 77 K with an automatic gas sorption system: Quantasorb EVO/SI from Quantachrome Instruments (Anton Paar). The samples were degassed under vacuum at 150 – 250 °C for 4 – 12 hr before the sorption measurements. The surface area was determined using 5 points BET (Brunauer-Emmett-Teller) method, and the BJH (Barrett-Joyner-Halenda) method was used for pore volume and pore size distribution determination. Diffuse Reflectance Infrared Fourier Transform Spectroscopy (DRIFTS) was used to study the nature of Pt species in these catalysts. A Tensor 27 spectrometer (Bruker) equipped with a DRIFTS cell (Harrick Scientific Inc.) was employed. For pre-treatment, samples (in the powder form) were loaded in the DRIFTS

cell and heated at 350 °C in flowing 10% O_2 for 30 min and pure He for 20 min, consecutively. Afterwards, the sample cell was cooled down in He to 125 °C and the background spectrum was collected. Then the gas flow was switched to a lean CO oxidation stream (60 ml min^{-1}) consisting of 1% CO, 4% O_2, balanced with Helium. During the measurements, DRIFTS spectra were collected in absorption mode every 1 min with a resolution of 4 cm^{-1}. The ramp rate for heating up and cooling down during all the measurements was 20 °C min^{-1}. In another experiment, after collecting a stable spectrum under CO oxidation conditions for 30 min, CO and O_2 were stopped, and the spectra were collected under He flow for 10 min. Afterward, O_2 was switched on again to investigate the reaction of the adsorbed CO with flowing 4% O_2/He for 10 min.

Catalyst Testing

The Pt reactivity was measured using CO oxidation as a probe reaction, under flowing CO (1.5 cm^3(STP) min^{-1}), O_2 (1 cm^3(STP) min^{-1}) and He (75 cm^3(STP) min^{-1}) conditions in a quartz tube. Reactivity measurements for each catalyst sample (20 mg) were carried out from 25 to 300 °C (2 °C/min ramp rate). After the first run, the sample was cooled to room temperature in the reaction mixture, and the second activity measurement was carried out to 300 °C. Triplicate runs were performed to determine the stability of the Pt catalysts, the third run is reported, but the results were quite consistent among the three runs. The sample was then reduced in-situ under flowing CO (5.0 cm^3(STP) min^{-1}) and He (75 cm^3(STP) min^{-1}) conditions at 275 °C for 1 hr followed by another set of triplicate CO oxidation runs, with the third run also reported. The reactor effluent was analyzed by a micro GC (Varian CP-4900).

Results and Discussion

Characterization and thermal stability of ceria/alumina supports

The AC-STEM images of the CA08 ceria/alumina are shown in Fig. 1. The CA08 support contains ceria crystallites (Fig. 1a) and atomically dispersed Ce (Figure 1b). Table 1 shows the XRD and EDS quantification, BET surface area, and pore volume of the supports, as well as an estimate of the surface area of ceria. Since the surface area of ceria cannot be directly measured on the ceria/alumina supports by BET, we estimated the surface area using the equation $6/\rho d$, where ρ is the density of ceria and d is the XRD-derived average crystallite size and multiplying this number by percent ceria in ceria/alumina. For example, in the CA08 sample, with a crystallite size of 77 A, we would expect a BET surface area of 109 m^2/g. Since the ceria content is 7.8 wt%, this translates to 9 m^2/g of ceria surface area as reported in Table 1. This estimate assumes spherical ceria particles, with no agglomeration, but ignores any surface roughness. Hence, this calculation generally underestimates the measured surface area in ceria powders. It is provided here as an indication of the effective surface area of ceria provided by the ceria/alumina powder samples.

We performed EDS analysis of sample CA08 at low magnifications, to determine total ceria loading, and we analyzed regions devoid of ceria crystallites to determine the loading of cerium in atomically dispersed form on the alumina support (Fig. 1b). Overall EDS analysis showed significant variability, ranging from 8.8 to 20.1 wt%, reflecting the heterogeneity of this sample. This variability is consistent with the non-uniform distribution of ceria crystallites on the alumina (see Fig. S1), which is why we

cannot use this EDS analysis to derive total ceria loading. EDS analysis is reliable when the sample is uniform, otherwise it is difficult to derive an average metal loading. To confirm the overall loading of ceria, we therefore performed ICP-OES analysis of this sample which showed the loading to be 7.8 wt% ceria on alumina, which is consistent with the nominal loading reported by the manufacturer. In our previous work [6], we used whole pattern fitting and quantitative XRD analysis to determine the fraction of crystalline Pt on ceria and alumina physical mixtures. Here we applied a similar approach to derive the wt% of crystalline ceria on alumina. Fig. S2 shows XRD patterns of the ceria/alumina samples as received and after 800 °C treatment in air. The powder patterns show that the ceria reflections increase in intensity as the ceria content of the sample increases. The results of the quantitative XRD analysis are presented in Table 1 which show that the estimated amount of ceria present in crystalline form is 5.6 wt% on the CA08 sample. If we subtract the amount of crystalline ceria (5.6 wt%) from the total ceria in the sample (7.8 wt%) we infer that 2.2 wt% of ceria might be present in the form of single atoms. Our spot EDS analysis shows the presence of atomically dispersed Ce present on the sample (Fig. 1b). These isolated cerium atoms are also visible at high magnifications in AC-STEM images. Both the EDS small area analysis and the XRD quantification are consistent with the presence of atomically dispersed cerium being present on this sample in addition to the ceria crystallites seen via XRD and the AC-STEM.

AC-STEM images of the CA30 and CA50 supports are shown in Fig. 2 and Fig. 3, respectively. Both supports contain ceria crystallites and atomically dispersed cerium on alumina. These samples are more uniform than CA08 and the margin of error for CA30 and CA50 was ± 0.9 and ± 0.5 wt% respectively, suggesting that ceria is uniformly dispersed on the alumina. By performing EDS analysis at low magnification, which accounts for all the ceria present, we find the ceria loading to be 29.4 wt% in CA30 and 53.8 wt% in CA50. This loading is consistent with the values reported by the manufacturer. By using the same quantitative XRD analysis used for sample CA08, we find that these samples contain 23.2 wt% ceria in crystalline form in CA30 and 47.5 wt% in CA50. By difference, we would infer that these samples contain 6.2 wt% Ce (29.4 wt% - 23.2 wt%) in single atom form on CA30 and 6.3 wt% Ce (53.8 wt% - 47.5 wt%) in single atom form on CA50. When we perform EDS analysis of regions devoid of ceria crystallites, we detect 5.5 ± 1.6 wt% and 8.4 ± 3.9 wt% cerium to be present in atomically dispersed form in CA30 and CA50, respectively. In view of the uncertainties in the methods used to derive the loading of crystalline and atomically dispersed species, we conclude that both samples contain significant concentrations of atomically dispersed Ce, as seen also via AC-STEM images (Fig. 2 and 3).

Besides determining the amount of crystalline ceria, the XRD patterns of the three ceria/alumina supports also provide information on lattice constant and crystallite sizes, before and after 800 °C treatment in air for 10 h. This heat treatment causes modest growth in ceria crystallite size in sample CA08 (increasing from 7.7 nm to 8.7 nm) but a more significant ceria sintering in samples CA30 and CA50 with final crystallite sizes of 5.6 nm and 7.8 nm, respectively. The BET surface area of these samples also decreases after the thermal treatment, from 147 m^2/g to 126 m^2/g for CA08, and similar declines for the other ceria/alumina samples. We compared the characteristics of the ceria/alumina samples with polyhedral ceria prepared via decomposition of cerium nitrate. Fig. S3 shows the XRD patterns of the as-prepared polyhedral ceria, after heating at 800 °C in air for 5 hr and after heating 1 wt% Pt/polyhedral ceria for 5 hr also at 800 °C in air. In our previous work, we showed that after heating polyhedral ceria at 800 °C, BET surface area significantly decreased from 83 to 5 m^2/g (Table

1), with an increase in crystallite size to 53.6 nm [8]. This leads to the significant sharpening of the ceria reflections in Fig. S3. In contrast, Pt helps to slow the sintering of the ceria and likewise ceria helps to stabilize atomically dispersed Pt since we do not see any Pt XRD reflections after heating in air. It is evident that sintering of ceria occurs to a much lesser extent in the ceria/alumina supports (Fig. S2), with alumina helping to stabilize ceria when heating at high temperatures. In turn, atomically dispersed cerium may help to minimize phase transformation of γ-Al_2O_3 when heated to temperatures above 800 °C, which is important for DOCs in maintaining high surface area and dispersion of PGMs. The high concentration of Ce atoms on the alumina support may play an important role. Since the mechanism of ceria sintering likely involves surface diffusion of ceria, with the surface sites on alumina occupied, it will reduce the driving force for Ostwald ripening. Likewise, the isolated Ce atoms may pin the alumina surface sites and retard the phase transformation and sintering of alumina, just like atomically dispersed La [11-15].

Fig. S4 shows AC-STEM images of CA13, which was prepared in our laboratory. This ceria/alumina clearly shows both ceria crystallites (Fig. S4a) and atomically dispersed cerium on alumina (Fig. S4b), with a morphology very similar to the commercial CA30 and CA50 samples. In contrast to CA30 and CA50, we find both samples CA13 and CA08 show variability in overall EDS ceria loading, which is likely a result of the lower ceria loading. For CA13 we find the overall loading to be 9.0 ± 2.5 wt%, and ~1.3 wt% of cerium is in atomically dispersed form. This characterization demonstrates that the ceria/alumina prepared in the laboratory is very similar to the commercial ceria/alumina samples that were used in this study.

Trapping of Pt single atoms on ceria/alumina

The efficacy of the ceria/alumina samples for trapping Pt in atomically dispersed form was studied by heating the samples in air at 800 °C for 10 h. The catalysts prepared via atom trapping are designated with the 'AT' subscript symbol followed by the support (CA08, CA13, CA30, CA50, or polyhedral ceria PHC). XRD patterns of the 1 wt% Pt_{AT}/ceria-alumina catalysts are shown in Fig. 4. As we showed previously, any Pt not atomically trapped on ceria forms abnormally large particles [7, 16], hence is readily visible via XRD. The height of the Pt(111) and Pt(200) peaks decreases from CA08 to CA50, suggesting improved efficiency for atom trapping Pt (since the XRD visible portion of Pt is decreasing) despite identical Pt loading. The ceria/alumina supports, however, are not 100% efficient for atom trapping Pt compared to pure ceria supports (see the complete absence of a Pt reflection on the 1 wt% Pt_{AT}/PHC ceria here and in Fig. S3) [6]. Table 2 shows the XRD, BET surface area and pore volume properties of the Pt/ceria-alumina catalysts and Pt_{AT}/PHC. N_2 isotherms and pore size distributions are shown in Fig. S5. Using XRD Rietveld refinement to quantify the crystalline Pt phase, we estimate the metallic Pt loading after 800 °C heating in air to be 1.03 wt% on CA08, 0.60 wt% on CA30 and 0.2 wt% on CA50 with no crystalline Pt visible on the PHC ceria. Since the nominal Pt loading is 1 wt%, there should be no single Pt atoms in Pt_{AT}/CA08, 0.4 wt% single Pt atoms in Pt_{AT}/CA30, 0.8 wt% single Pt atoms in Pt_{AT}/CA50 and 1 wt% single Pt atoms on PHC ceria. Based on the measured BET surface area, we can estimate the surface atom concentration of Pt_{AT}/PHC to be 1.1 Pt atoms/nm^2 which is consistent with the upper limit we obtained on Pt/ceria [7]. If we consider the estimated surface area of ceria shown in Table 1 and the Pt in single atom form, the estimated surface atom concentration of the Pt/ceria-alumina catalysts is in the range of 0.28 – 0.47 Pt atoms/nm^2. With hemispherical particles of ceria, if we assume only 50% of the surface area is available for atom trapping, it suggests that a

saturation coverage of ~1 atom Pt/nm^2 is reached in the CA50 sample. This would explain the presence of Pt nanoparticles to differing extent on all the ceria/alumina samples.

Fig. 5 shows AC-STEM images of the Pt_{AT}/CA50 catalysts. The boxes shown in the figure indicate regions from where we obtained EDS spectra. Regions devoid of ceria crystallites show no Pt (B and C), whereas ceria crystallites contain 0.6 – 0.8 wt% Pt (A and D), but no Pt nanoparticles are visible. The Pt detected on the crystalline ceria phase is close to the estimate of 0.8 wt% Pt as single atoms based on the difference between the total Pt loading and the Pt detected via XRD. Polyhedral ceria particles exhibit surface step sites on CeO_2(111) where, in our previous work, we have found under-coordinated Ce^{3+} cations capable of reacting with mobile PtO_2 species [7]. The oxygen atoms provided by the Pt are shared with Ce^{3+} cations to form strong covalent bonds, which trap the ionic Pt species and retain them in atomically dispersed and thermally stable form. In the case of atomically dispersed cerium on alumina, cerium is likely present as Ce^{3+} cations which might be expected to help stabilize Pt^{2+}. However, the isolated nature of the Ce^{3+} may not allow formation of the four-fold surface complex, which is needed to stabilize atomically dispersed Pt. Heating at 800 °C in air for 10 hr is a very demanding test and only strongly bound Pt surface complexes will survive. These results demonstrate that such sites are only present on the ceria crystallites, and hence the CA50 sample is more effective for atom trapping Pt than CA30 due to the larger availability of ceria crystallites in CA50. These images show clearly the presence of atomically dispersed Ce which persists after high temperature treatments, suggesting that analogous to the atomically dispersed La^{3+} cations on alumina [11-14, 17], the dispersed Ce may also help in thermally stabilizing alumina at high temperatures against sintering and phase transformation.

The Pt/ceria-alumina samples were imaged using AC-STEM to verify the formation of large Pt particles. For the Pt_{AT}/CA08 catalyst, Fig. 6 shows large Pt particles (approaching 100 nm in size) which we did not see in Pt_{AT}/CA30 and Pt_{AT}/CA50 by AC-STEM. Although crystalline Pt was found by XRD in all three catalysts and the average Pt crystallite sizes were large enough that they should be easy to image, it is often difficult to find the few large Pt particles that may be present. The sum of crystalline Pt via XRD data and atom trapped Pt via AC-STEM/EDS gives us the total Pt content, allowing us to complete the mass balance for Pt. Within the margin of error, the total Pt content in Pt_{AT}/CA50 and Pt_{AT}/CA30 is close to 1 wt%. Fig. 7 shows higher magnification views of Pt_{AT}/CA08, demonstrating that while the crystalline ceria can trap Pt in atomically dispersed form, with a much smaller ceria loading, most of the Pt is present in the form of metallic nanoparticles.

For the Pt_{AT}/CA13 catalyst, Fig. S6a also shows large Pt particles similar to what we see in Pt_{AT}/CA08 (Fig. 6). By XRD, Pt in crystalline form is 0.8 wt% on CA13 lying between the 1.03 wt% on CA08 and 0.60 wt% on CA30 (Table 2). If the nominal Pt loading is 1 wt%, there should be 0.2 wt% single Pt atoms in Pt_{AT}/CA13. As expected, Fig. S6b shows that regions devoid of ceria crystallites show no Pt, whereas ceria crystallites show 0.1 – 0.7 wt% Pt. On average, by EDS the wt% Pt detected on the crystalline ceria phase is 0.3 wt%, which is close to the estimate of 0.2 wt% Pt as single atoms based on the difference between the total Pt loading and the Pt detected via XRD and this is also consistent with the CO-DRIFTS as we show next.

CO-DRIFTS of the Pt catalysts

Diffuse reflectance infrared Fourier transform spectroscopy (DRIFTS) using CO as a probe molecule was employed to probe the nature of Pt supported on different ceria/alumina supports. CO-DRIFTS was used instead of CO pulse chemisorption due, in part, to the oxidized form of Pt which adsorbs CO weakly [18]. Furthermore, CO can reduce the Pt and react with ceria, making CO chemisorption unreliable as a probe for Pt dispersion on the as-prepared atom trapped Pt samples on ceria. For CO-DRIFTS, all catalysts were tested under lean CO oxidation (1% CO, 4% O_2) at 125 °C. The spectra after 30 min CO oxidation were summarized, normalized by the gaseous CO absorption peak at 2174 cm^{-1}. As shown in Fig. 8, all samples only showed a peak located around 2090 cm^{-1}, which we assign to CO adsorbed on isolated Pt^{2+} cations (i.e., Pt single atoms) [6, 7, 19]. We recognize that other authors have reported CO-IR bands assigned to CO-Pt isolated species in Pt/ceria, ranging from 2088 cm^{-1} to 2095 cm^{-1} [20-23]. It has also been suggested that definitive assignment of the adsorbed CO band can only be performed with samples that have very low Pt loading (0.05 wt%) since higher loadings can lead to formation of sub-nanometer clusters [24]. Meunier [25] has described the challenges in unambiguously assigning IR bands. We note that our assignment of the band in Figure 8 is based not just on the peak position but the physical characteristics of the CO band. CO linearly adsorbed on extended Pt surfaces (e.g., Pt/PtO_x clusters/NPs) shows blueshifts with increased CO coverage due to the dipole coupling (or repulsive interaction) of CO molecules. This has been extensively confirmed in real catalysts as well as model catalysts [26, 27], i.e., redshifts of CO-Pt NPs will be observed upon CO desorption due to the decreased CO coverage. We studied the effect of coverage by allowing the CO to desorb by flushing the catalyst with He and He/O_2 for two of the catalysts. Fig. S7 shows that for Pt_{AT}/PHC and Pt_{AT}/CA50, the well-defined ~2090 cm^{-1} peak shows no shift in peak position upon He/O_2 purging. Since the 2090 cm^{-1} peak on these samples cannot be reacted by O_2 even at 120 °C, it suggests that this peak does not come from Pt NPs/clusters where the adsorbed CO can be readily reacted in O_2 once CO flow is stopped. Furthermore, we can rule out partially oxidized Pt clusters since they will show CO-IR bands above 2100 cm^{-1} [23], which is supported by DFT calculations. In addition, the absence of any Pt clusters on the ceria crystallites supports our assignment of the strongly bound CO feature as arising from atomically dispersed Pt.

The strongly bound CO feature on the single atom catalysts may seem surprising since previous studies suggested via DFT that square planar Pt_1O_4 provides very weak binding to CO [28, 29]. Our observations of strongly bound CO are not inconsistent with this finding, since we have also previously confirmed that CO-Pt_1 band is very weak at room temperature. In fact, room temperature CO-chemisorption showed that the ratio between adsorbed CO and loaded Pt atoms was only 3% [21]. Surprisingly, the 2090 cm^{-1} peak height increased with temperature, indicating increased CO adsorption on Pt_1. We proposed this was due to the transformation of Pt_1O_4 to Pt_1O_3 as supported by DFT [18]. The 2090 cm^{-1} peak arises from isolated Pt species, supported by STEM images showing the absence of clusters/nanoparticles in the spent catalyst and EXAFS. It should be noted all our CO-DRIFTS data are obtained at elevated temperature (e.g., 120 °C) under lean CO oxidation which avoids Pt_1 reduction/sintering.

The CO-Pt^{2+} peak intensity decreased in the order Pt_{AT}/CA50 > Pt_{AT}/PHC > Pt_{AT}/CA13 > Pt_{AT}/CA08, indicating that the concentration of isolated Pt atoms in these samples decreased in the same order. As ceria loading decreased in the ceria/alumina supports, the trapping of isolated Pt atoms was less efficient, resulting in the decreased CO-Pt^{2+} peak intensity. Since no metallic Pt XRD peak was seen on the PHC ceria, we can assume the entire 1 wt% of Pt atoms was present in the form of isolated Pt species. In contrast, our estimate was 0.8 wt% single Pt atoms on CA50, which showed a more prominent CO peak. Compared to PHC, which sintered during the atom trapping process, a small amount of Pt may be buried in the PHC ceria, resulting in less surface exposure of Pt atoms and the smaller CO band on this sample.

None of these samples showed lower wavenumber IR features (~ 2080 and < 2000 cm^{-1}) which are characteristic of CO adsorption on Pt nanoparticles [19, 21, 30] despite the clear detection of an XRD peak due to metallic Pt. We reported a similar absence of the IR band for Pt nanoparticles in 4 wt% Pt/ceria which had a metal loading in excess of the single atom limit, leading to a co-existence of single atoms and large Pt particles [7]. This was explained by the presence of very large Pt particles, which are also seen in these samples (Fig. 6). The low surface area of these large Pt particles may make them difficult to detect by via CO-DRIFTS. To demonstrate the absence of smaller metallic Pt clusters in these samples, we treated the Pt_{AT}/CA13 in CO at 275 °C (Fig. S8) to cause a transformation of the single atoms into metallic nanoparticles. The IR spectra now show bands characteristic of CO adsorbed to metallic Pt, with a small residual CO-Pt^{2+} peak. After purging in He/O_2, CO adsorbed on Pt nanoparticles was readily reacted away, showing a clear difference compared to the stability of the 2090 cm-1 band (Fig. S7). This confirms that the CO-DRIFTS features shown in Fig. 8 arise from single atom Pt species atomically trapped on the ceria and not from metallic clusters of Pt.

CO Oxidation as a probe for atom trapping of Pt

CO oxidation was used as a probe reaction to evaluate the performance of the Pt catalysts prepared via atom trapping. This is based on previous work [19, 31] that shows that atom trapping creates the precursor to the active catalyst. When the Pt is converted into nanoparticles, we see excellent low temperature reactivity. The dramatic shifts in CO oxidation reactivity serve as a probe for the presence of isolated single atom Pt sites on the ceria. Using this approach, we studied the reactivity of the as-prepared (calcined and oxidized) catalyst and after reduction in flowing CO at 275 °C. For each catalyst, we performed three runs. Both in the as-prepared state and after reduction, the CO oxidation performance is reproducible over multiple runs. To illustrate this, we report the results of the first and third runs on a reduced catalyst in Fig. S9. Fig. S10 shows that all the catalysts show low reactivity in the as-prepared atom trapped state and excellent low temperature reactivity after reduction in CO. The enhancement in reactivity can be seen very clearly in the Arrhenius plots for CO oxidation, shown in Fig. S11. The greatest degree of enhancement in reactivity upon reduction is seen on the Pt/PHC sample, which has all the Pt in atomically dispersed form. In the low temperature region, this is the most active catalyst.

The performance of the reduced catalysts is shown in Fig. 9, once again for the third run (RT to 300 °C) in a lean mixture (excess oxygen). These catalysts show onset of CO oxidation reactivity near room temperature. This is surprising since it is well known that CO adsorbs strongly on metallic Pt, leading to low reactivity below the desorption temperature of CO. As we have shown

recently, on the reduced Pt/ceria prepared via atom trapping, the enhancement in low temperature CO oxidation reactivity [32] is due to facile oxygen transfer from the ceria support and not due to any changes in the CO binding energy. The temperature to achieve 90% conversion of CO is regarded as a measure of the performance of the catalyst. The T_{90} for Pt_{AT}/CA50, Pt_{AT}/PHC, Pt_{AT}/CA30, Pt_{AT}/CA08, and Pt_{AT}/CA13 is 120 °C, 138 °C, 160 °C, 206 °C, and 215 °C, respectively. The differences in activity (lower light-off temperature) can be correlated with the area of the DRIFTS peak for adsorbed CO. The most active catalyst (lowest T_{90}) had the largest adsorbed CO peak in Fig. 8, indicating the highest concentration of trapped Pt atoms. Surprisingly, the pure ceria sample does not exhibit the lowest T_{90}, suggesting that the ceria/alumina samples outperform the pure ceria. This could be a result of the differences in physical characteristics such as BET surface area and might also suggest that the close proximity of the ceria and alumina may be beneficial in this reaction.

Conclusions

In this study, we examined ceria/alumina supports with increasing ceria content (CA08, CA13, CA30, CA50) to assess their ability to trap Pt atoms compared to pure ceria prepared by decomposition of cerium nitrate (polyhedral ceria). All ceria/alumina supports contained crystalline ceria as well as isolated cerium cations dispersed on alumina, but the two forms of ceria differed remarkably in their ability to trap Pt atoms. The atom trapped Pt resided primarily on the ceria crystallites, whereas the atomically dispersed cerium present in the form of Ce^{3+} cations on alumina was not effective for trapping Pt atoms, at least not at 800 °C in air. Using CO oxidation as a probe reaction to evaluate the performance of the Pt catalysts, CA50 was the best catalyst support for achieving very good low temperature reactivity for the Pt catalyst. The ceria/alumina samples retained small crystallite sizes helping preserve a high surface area compared to pure ceria, which lost almost all its surface area after heating at 800 °C in air. However, in terms of atom trapping efficiency, pure crystalline ceria was the most effective, despite having a lower surface area and larger crystallite size. The work suggests that just the presence of Ce^{3+} cations is not sufficient for atom trapping, the extended surface is needed to allow Pt to form the stable four-fold complex. Our work also suggests that the smallest ceria crystallites in CA08 provide the greatest thermal stability, since the ceria phase in CA08 sample did not show significant sintering or particle growth after heating to 800 °C in air for 10 hr. From the viewpoint of developing sustainable emission control catalysts with the lowest rare-earth loading, we see 50% ceria as the optimal sample since its performance after depositing Pt exceeds that of pure ceria.

Supporting Information. The Supporting Information is available free of charge.

AC-STEM images of CA08 and CA13 supports, and Pt_{AT}/CA13 catalyst; XRD patterns of ceria/alumina and polyhedral ceria supports; N_2 isotherms and pore size distributions of Pt_{AT}/ceria-alumina catalysts; additional CO-DRIFTS, CO oxidation and Arrhenius plots of Pt_{AT}/ceria-alumina and Pt_{AT}/polyhedral ceria catalysts.

Acknowledgement The manuscript is submitted as part of a special virtual issue honoring of Prof. Dumesic's distinguished career. The authors (HNP and AKD) thank Prof. James Dumesic for many years of collaborations, advice and for sharing his insights in catalyst synthesis and heterogeneous catalysis. Financial support for the catalyst synthesis and characterization was provided by the U.S.

Department of Energy (DOE), Energy Efficiency and Renewable Energy (EERE), Vehicle Technologies Office (DE-FOA-0002197). The study of ceria doping was supported by the NSF/ERC CISTAR under Cooperative Agreement No. EEC-1647722. Acquisition of the TEM was supported by the NSF MRI grant DMR-1828731. Fundamental studies of atom trapping were supported by the DOE/BES Catalysis Science program, grant DE-FG02-05ER15712.

References

1. Wang, A. and Olsson, L., *The impact of automotive catalysis on the United Nations sustainable development goals.* Nat. Catal., 2019. **2**(7): p. 566-570. Doi.org/10.1038/s41929-019-0318-3
2. Lambert, C.K., *Current state of the art and future needs for automotive exhaust catalysis.* Nat. Catal., 2019. **2**(7): p. 554-557. Doi.org/10.1038/s41929-019-0303-x
3. Rappé, K.G., DiMaggio, C., Pihl, J.A., Theis, J.R., Oh, S.H., Fisher, G.B., Parks, J., Easterling, V.G., Yang, M., Stewart, M.L., and Howden, K.C, *Aftertreatment Protocols for Catalyst Characterization and Performance Evaluation: Low-Temperature Oxidation, Storage, Three-Way, and NH3-SCR Catalyst Test Protocols.* Emission Contr. Sci. Technol., 2019. **5**(2): p. 183-214. Doi.org/10.1007/s40825-019-00120-7
4. *Future Automotive Aftertreatment Solutions: The 150˚C Challenge Workshop Report (US Department of Energy, 2012),* https://cleers.org/wp-content/uploads/2012_The_150C_Challenge_Workshop_Report.pdf*, last accessed on Mar. 7, 2022.* Doi.org/10.2172/1097340
5. Kang, S.B., Lim, J.B., Jo, D., Nam, I.-S., Cho, B.K., Hong, S.B., Kim, C.H., and Oh, S.H., *Ostwald-ripening sintering kinetics of Pd-based three-way catalyst: Importance of initial particle size of Pd.* Chem. Eng. J., 2017. **316**: p. 631-644. Doi.org/10.1016/j.cej.2017.01.136
6. Jones, J., Xiong, H., DeLaRiva, A.T., Peterson, E.J., Pham, H., Challa, S.K., Qi, G., Oh, S., Wiebenga, M.H., Hernandez, X.I.P., Wang, Y., and Datye, A.K., *Thermally stable single-atom platinum-on-ceria catalysts via atom trapping.* Science, 2016. **353**(6295): p. 150-154. DOI: 10.1126/science.aaf8800
7. Kunwar, D., Zhou, S., DeLaRiva, A., Peterson, E.J., Xiong, H., Pereira-Hernandez, X.I., Purdy, S.C., ter Veen, R., Brongersma, H.H., Miller, J.T., Hashiguchi, H., Kovarik, L., Lin, S., Guo, H., Wang, Y., and Datye, A.K., *Stabilizing High Metal Loadings of Thermally Stable Platinum Single Atoms on an Industrial Catalyst Support.* ACS Catal., 2019. **9**(5): p. 3978-3990. Doi.org/10.1021/acscatal.8b04885
8. Alcala, R., DeLaRiva, A., Peterson, E.J., Benavidez, A., Garcia-Vargas, C.E., Jiang, D., Pereira-Hernández, X.I., Brongersma, H.H., Veen, R.t., Staněk, J., Miller, J.T., Wang, Y., and Datye, A., *Atomically Dispersed Dopants for Stabilizing Ceria Surface Area.* Appl. Catal., 2021. **284**: Article 119722. Doi.org/10.1016/j.apcatb.2020.119722
9. Jeong, H., Kwon, O., Kim, B.-S., Bae, J., Shin, S., Kim, H.-E., Kim, J., and Lee, H., *Highly durable metal ensemble catalysts with full dispersion for automotive applications beyond single-atom catalysts.* Nat. Catal., 2020. **3**(4): p. 368-375. Doi.org/10.1038/s41929-020-0427-z
10. Xie, S., Wang, Z., Tan, W., Zhu, Y., Collier, S., Ma, L., Ehrlich, S.N., Xu, P., Yan, Y., Xu, T., Deng, J., and Liu, F., *Highly Active and Stable Palladium Catalysts on Novel Ceria-Alumina Supports for Efficient Oxidation of Carbon Monoxide and Hydrocarbons.* Environ. Sci. Technol., 2021. **55**(11): p. 7624-7633. Doi.org/10.1021/acs.est.1c00077
11. Ozawa, M. and Nishio, Y.. *Thermal stabilization of gamma-alumina with modification of lanthanum through homogeneous precipitation*. J. Alloys Compd., 2004. **374**(1-2): p. 397-400. Doi.org/10.1016/j.jallcom.2003.11.032

12. Ozawa, M. and Nishio, Y., *Thermal stability and microstructure of catalytic alumina composite support with lanthanum species.* Appl. Surf. Sci., 2016. **380**: p. 288-293. Doi.org/10.1016/j.apsusc.2015.12.246
13. Beguin, B., Garbowski, E., and Primet, M., *Stabilization Of Alumina By Addition Of Lanthanum.* Appl. Catal., 1991. **75**(1): p. 119-132. Doi.org/10.1016/S0166-9834(00)83128-0
14. Chen, X., Liu, Y., Niu, G., Yang, Z., Bian, M., and He, A., *High temperature thermal stabilization of alumina modified by lanthanum species*. Appl. Catal. A: Gen., 2001. 205(1-2): p. 159-172. Doi.org/10.1016/S0926-860X(00)00575-5
15. Peterson, E.J., Delariva, A.T., Lin, S., Johnson, R.S., Guo, H., Miller, J.T., Kwak, J.H., Peden, C.H.F., Kiefer, B., Allard, L.F., Ribeiro, F.H., and Datye, A.K., *Low-temperature carbon monoxide oxidation catalysed by regenerable atomically dispersed palladium on alumina.* Nat. Commun., 2014. **5**: Article 4885. Doi.org/10.1038/ncomms5885
16. Kunwar, D., Carrillo, C., Xiong, H., Peterson, E., DeLaRiva, A., Ghosh, A., Qi, G., Wiebenga, M., Oh, S., Li, W., and Datye, A.K., *Investigating anomalous growth of platinum particles during accelerated aging of diesel oxidation catalysts.* Appl. Catal., 2020. **266**: Article 118598. Doi.org/10.1016/j.apcatb.2020.118598
17. Haack, L.P., deVries, J.E., Otto, K., and Chattha, M.S., *Characterization of lanthanum-modified γ-alumina by X-ray photoelectron spectroscopy and carbon dioxide absorption.* Appl. Catal. A: Gen., 1992. **82**(2): p. 199-214. Doi.org/10.1016/0926-860X(92)85005-V
18. Lu, Y., Zhou, S., Kuo, C.-T., Kunwar, D., Thompson, C., Hoffman, A.S., Boubnov, A., Lin, S., Datye, A.K., Guo, H., and Karim, A.M., *Unraveling the Intermediate Reaction Complexes and Critical Role of Support-Derived Oxygen Atoms in CO Oxidation on Single-Atom Pt/CeO2.* ACS Catal., 2021. **11**(14): p. 8701-8715. Doi.org/10.1021/acscatal.1c01900
19. Hernandez, X.I.P., DeLaRiva, A., Muravev, V., Kunwar, D., Xiong, H., Sudduth, B., Engelhard, M., Kovarik, L., Hensen, E.J.M., Wang, Y., and Datye, A.K., *Tuning Pt-CeO2 interactions by high-temperature vapor-phase synthesis for improved reducibility of lattice oxygen.* Nat. Commun., 2019. **10**(1): p. 1-10. Doi.org/10.1038/s41467-019-09308-5
20. Wang, C., Mao, S., Wang, Z., Chen, Y., Yuan, W., Ou, Y., Zhang, H., Gong, Y., Wang., Y., Mei, B., Jiang, Z., and Wang, Y., *Insight into Single-Atom-Induced Unconventional Size Dependence over CeO2-Supported Pt Catalysts.* Chem, 2020. **6**(3): p. 752-765. Doi.org/10.1016/j.chempr.2019.12.029
21. Jiang, D., Yao, Y., Li, T., Wan, G., Pereira-Hernández, X.I., Lu, Y., Tian, J., Khivantsev, K., Engelhard, M.H., Sun, C., García-Vargas, C.E., Hoffman, A.S., Bare, S.R., Datye, A.K., Hu, L., and Wang, Y., *Tailoring the Local Environment of Platinum in Single-Atom Pt1/CeO2 Catalysts for Robust Low-Temperature CO Oxidation.* Angew. Chem. Int. Ed., 2021. **60**(50): p. 26054-26062. Doi.org/10.1002/anie.202108585
22. Maurer, F., Jelic, J., Wang, J., Ganzler, A., Dolcet, P., Woll, C., Wang, Y., Studt, F., Casapu, M., and Grunwaldt, J.-D., *Tracking the formation, fate and consequence for catalytic activity of Pt single sites on CeO2.* Nat. Catal., 2020. **3**(10): p. 824-833. Doi.org/10.1038/s41929-020-00508-7
23. Wang, H., Liu, J.-X., Allard, L.F., Lee, S., Liu, J., Li, H., Wang, J., Wang, J., OH, S.H., Li, W., Flytzani-Stephanopolos, M., Shen, M., Goldsmith, B.R., and Yang, M., *Surpassing the single-atom catalytic activity limit through paired Pt-O-Pt ensemble built from isolated Pt1 atoms.* Nat. Commun., 2019. **10**(1): Article 3808. Doi.org/10.1038/s41467-019-11856-9
24. Resasco, J., DeRita, L., Dai, S., Chada, J.P., Xu, M., Yan, X., Finzel, J., Hanukovich, S., Hoffman, A.S., Graham, G.W., Bare, S.R., Pan, X., and Christopher, P., *Uniformity Is Key in Defining Structure–Function Relationships for Atomically Dispersed Metal Catalysts: The Case of Pt/CeO2.* J. Am. Chem. Soc., 2020. **142**(1): p. 169-184. Doi.org/10.1021/jacs.9b09156

25. Meunier, F.C., *Relevance of IR Spectroscopy of Adsorbed CO for the Characterization of Heterogeneous Catalysts Containing Isolated Atoms.* J. Phys. Chem., 2021. **125**(40): p. 21810-21823. Doi.org/10.1021/acs.jpcc.1c06784
26. Rupprechter, G., Dellwig, T., Unterhalt, H., and Freund, H.-J., *High-Pressure Carbon Monoxide Adsorption on Pt(111) Revisited: A Sum Frequency Generation Study.* J. Phys. Chem., 2001. **105**(18): p. 3797-3802. Doi.org/10.1021/jp003585s
27. Qiao, B., Wang, A., Yang, X., Allard, L.F., Jiang, Z., Cui, Y., Liu, J., Li, J., and Zhang, T., *Single-atom catalysis of CO oxidation using Pt1/FeOx.* Nat. Chem., 2011. **3**(8): p. 634-641. Doi.org/10.1038/nchem.1095
28. Bruix, A., Lykhach, Y., Matolinova, I., Neitzel, A., Skala, T., Tsud, N., Vorokhta, M., Stetsovych, V., Sevcikova, K., Myslivecek, J., Fiala, R., Vaclavu, M., Prince, K.C., Bruyere, S., Potin, V., Illas, F., Matolin, V., Libuda, J., and Neyman, K.M., *Maximum Noble-Metal Efficiency in Catalytic Materials: Atomically Dispersed Surface Platinum.* Angew. Chem. Int. Ed., 2014. **53**(39): p. 10525-10530. Doi.org/10.1002/anie.201402342
29. Lykhach, Y., Figueroba, A., Farnesi Camellone, M., Neitzel, A., Skala, T., Negreiros, F.R., Vorokhta, M., Tsud, N., Prince, K.C., Fabris, S., Neyman, K.M., Matolin, V., and Libuda, J., *Reactivity of atomically dispersed Pt2+ species towards H2: model Pt–CeO2 fuel cell catalyst.* Phys. Chem. Chem. Phys., 2016. **18**(11): p. 7672-7679. Doi.org/10.1039/C6CP00627B
30. Xie, P., Pu, T., Nie, A., Hwang, S., Purdy, S.C., Yu, W., Su, D., Miller, J.T., and Wang, C., *Nanoceria-Supported Single-Atom Platinum Catalysts for Direct Methane Conversion.* ACS Catal., 2018. **8**(5): p. 4044-4048. Doi.org/10.1021/acscatal.8b00004
31. Ganzler, A.M., Casapu, M., Vernoux, P., Loridant, S., Cadete Santos Aires, F.J., Epicier, T., Betz, B., Hoyer, R., and Grunwaldt, J.-D., *Tuning the Structure of Platinum Particles on Ceria In Situ for Enhancing the Catalytic Performance of Exhaust Gas Catalysts.* Angew. Chem. Int. Ed., 2017. **56**(42): p. 13078-13082. Doi.org/10.1002/anie.201707842
32. Lu, Y., Thompson, C., Kunwar, D., Datye, A.K., and Karim, A.M., *Origin of the High CO Oxidation Activity on CeO2 Supported Pt Nanoparticles: Weaker Binding of CO or Facile Oxygen Transfer from the Support?* Chemcatchem, 2020. **12**(6): p. 1726-1733. Doi.org/10.1002/cctc.201901848

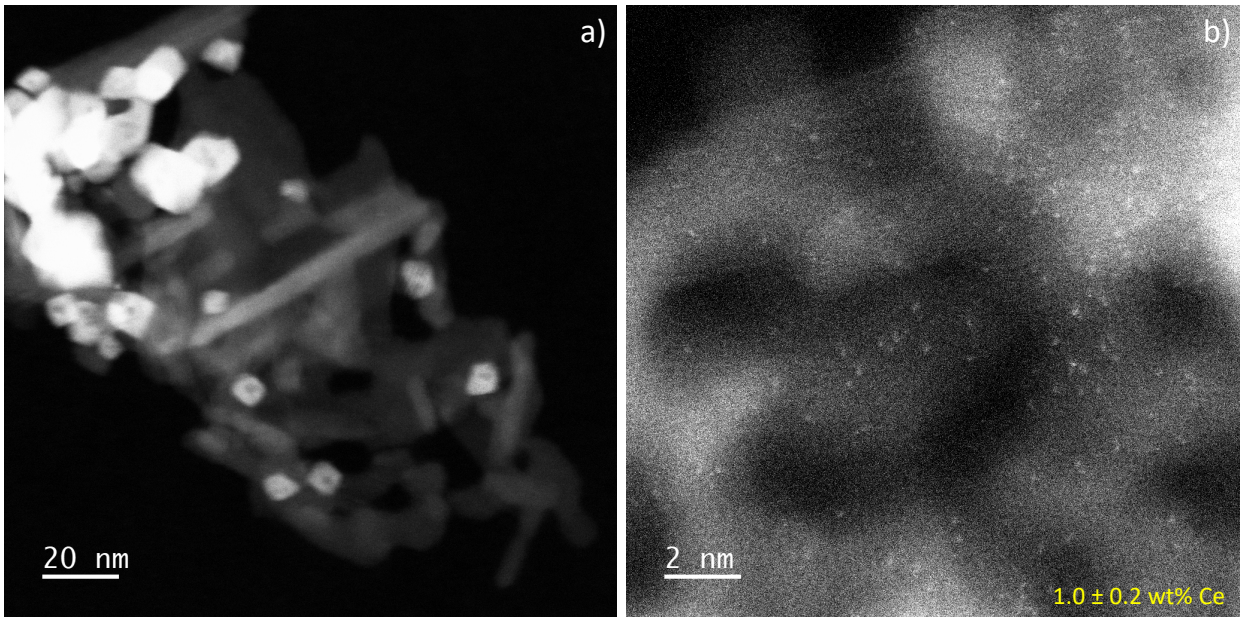

Fig. 1. AC-STEM images of CA08 showing a) ceria crystallites on the alumina. b) The region devoid of ceria crystallites shows a low concentration of Ce single atoms, and by EDS we find that the average loading is ~ 1.0 wt% atomically dispersed Ce cations (seen as bright dots) on alumina.

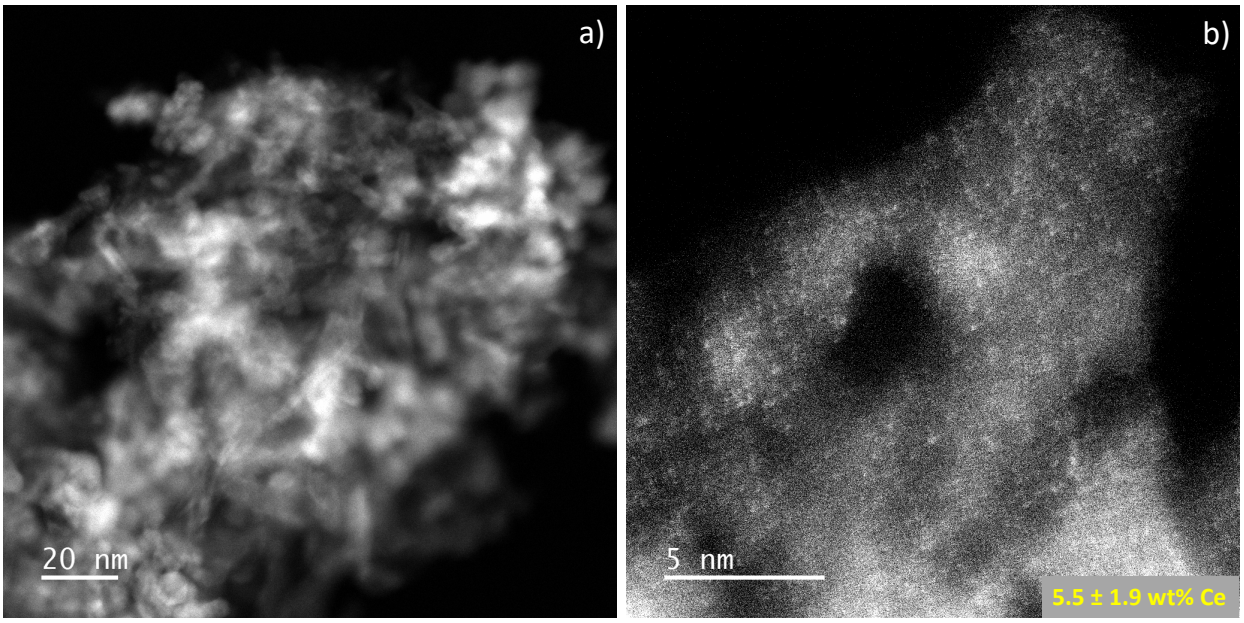

Fig. 2. AC-STEM images of CA30 showing a) ceria crystallites uniformly dispersed on the alumina. b) The region devoid of ceria crystallites shows a higher concentration of Ce single atoms, and by EDS we find that the average loading is ~ 5.5 wt% atomically dispersed Ce cations (seen as bright dots) on alumina.

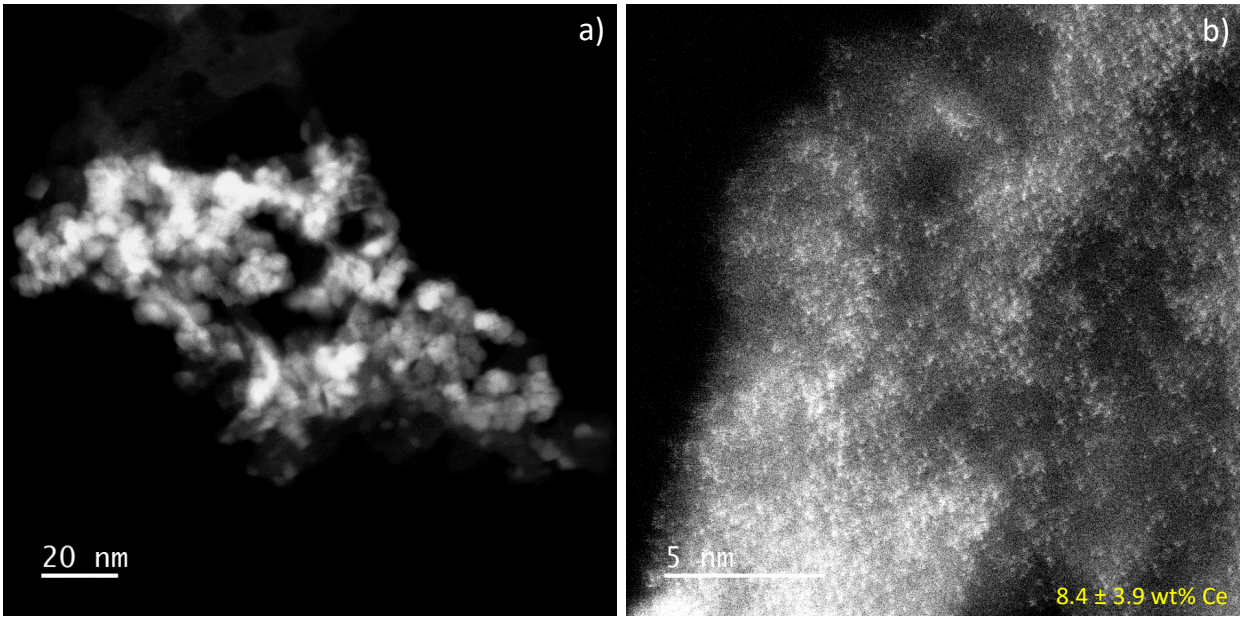

Fig. 3. AC-STEM images of CA50 showing a) a high concentration of ceria crystallites uniformly dispersed on the alumina. b) The regions devoid of crystallites show a higher concentration of single atoms of Ce (seen as bright dots), and by EDS the support has ~ 8.4 wt% atomically dispersed Ce on alumina.

Table 1. XRD, EDS, Surface Area and Pore Volume of Polyhedral Ceria and Ceria/Alumina

Samples	Crystalline Ceria by XRD (Wt%)	Ceria Crystallite Size (Å)	Lattice Constant (Å)	Ceria Loading (Wt%)	BET Surface Area (m^2/g)	Pore Volume (cc/g)	Surface Area of Ceria[a] (m^2/g)
CA08, As-Received	5.6	77	5.405	7.8	147	0.93	9
CA30, As-Received	23.2	38	5.411	29.4	190	1.12	66
CA50, As-Received	47.5	51	5.411	53.8	171	1.1	81
Polyhedral Ceria, As-Prepared	100	127	5.411	100	83	–	83
CA08, 800 °C, 10 hr, air	–	87	5.411	7.8	126	0.79	8
CA30, 800 °C, 10 hr, air	–	56	5.411	29.4	159	1.04	45
CA50, 800 °C, 10 hr, air	–	78	5.409	53.8	126	0.97	53
Polyhedral Ceria, 800°C, 5 hr, air	100	536	5.410	100	5	–	5

[a]Estimated using $6/\rho d$, where ρ is the density of ceria and d is the XRD derived crystallite size, and accounting for the wt% of ceria in the ceria/alumina supports. For pure ceria, we simply report the measured BET surface area.

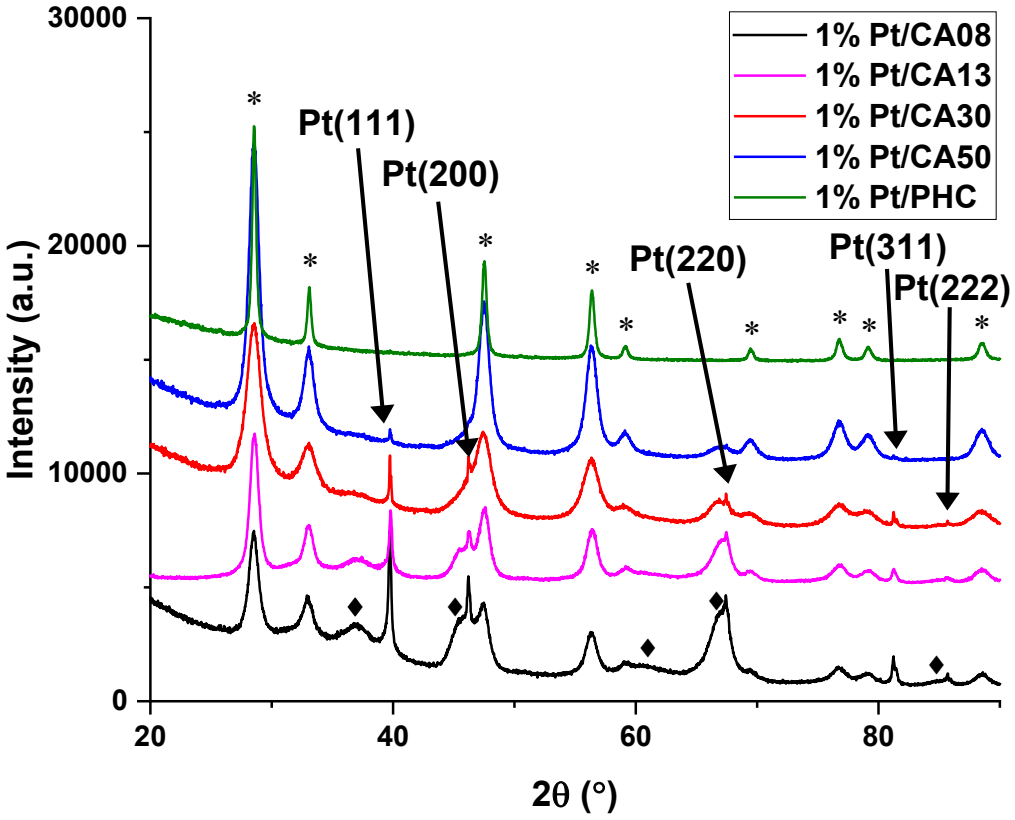

Fig. 4. XRD patterns of the 1 wt% Pt on ceria/alumina prepared using the atom trapping method (after heating in air for 10h at 800 °C). The ceria peaks are shown with (*) and belong to the fluorite structure of cerianite. The alumina reflections are marked with diamonds. The smaller the Pt peaks, more of the Pt is present in the form of single atoms. From the size of these peaks, it is evident that in sample CA08 the majority of Pt is present in the form of large crystals, with only a small fraction of Pt present in the form of single atoms, while in sample CA50 we see only a very small Pt peak since most of the Pt is present in the form of single atoms. Pt on polyhedral ceria shows no Pt peak indicating all the Pt is atomically dispersed.

Table 2. XRD, BET Surface Area and Pore Volume of 1 wt% Pt on PHC Ceria and Ceria/Alumina

Samples	Crystalline Pt (Wt%)	Pt Crystallite Size (nm)	Surface Area (m^2/g)	Pore Volume (cc/g)
1 wt% Pt_{AT}/CA08, 800 °C	1.03	40	128	0.65
1 wt% Pt_{AT}/CA13, 800 °C	0.80	31	–	–
1 wt% Pt_{AT}/CA30, 800 °C	0.60	96	161	0.89
1 wt% Pt_{AT}/CA50, 800 °C	0.20	89	121	0.90
1 wt% Pt_{AT}/PHC, 800 °C	Not Detected	Not Detected	26	–

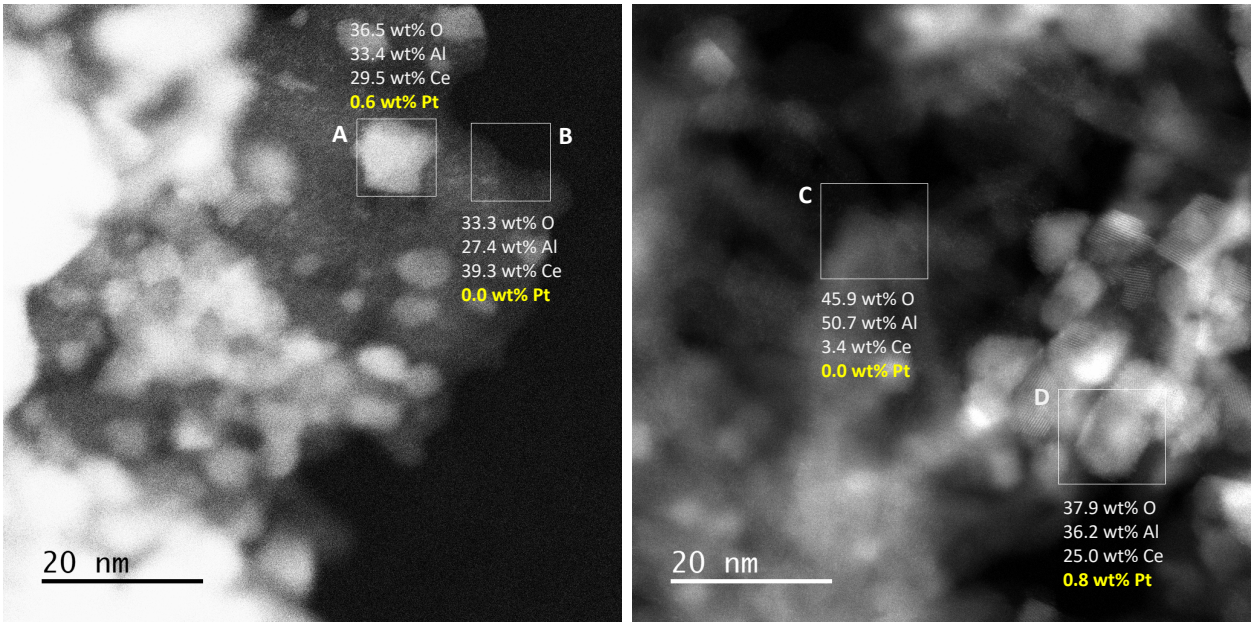

Fig. 5. AC-STEM images of the Pt_{AT}/CA50 catalyst. Regions A and D contain Pt atoms trapped on the ceria crystallites. Regions B and C are devoid of ceria crystallites and do not contain any Pt.

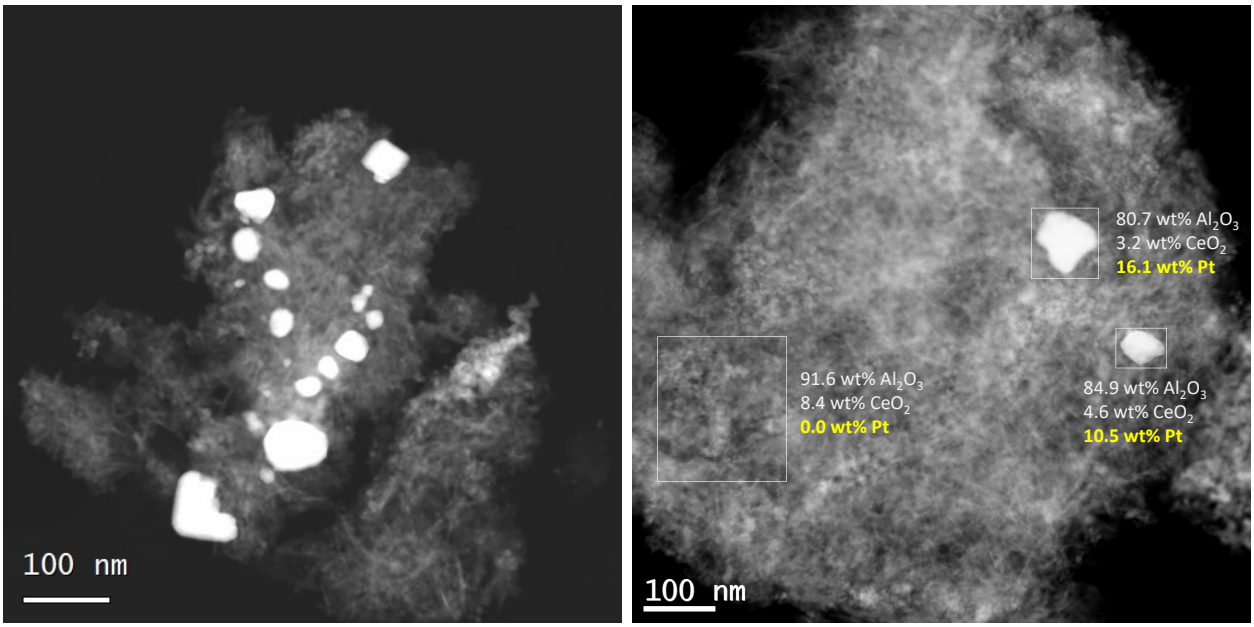

Fig. 6. AC-STEM images of the Pt_{AT}/CA08 catalyst showing the presence of large Pt particles, with little to no evidence for Pt via EDS in regions devoid of ceria crystallites. The ceria detected in the regions indicated in the boxes comes from the atomically dispersed Ce on the alumina, the bright objects are all large Pt particles.

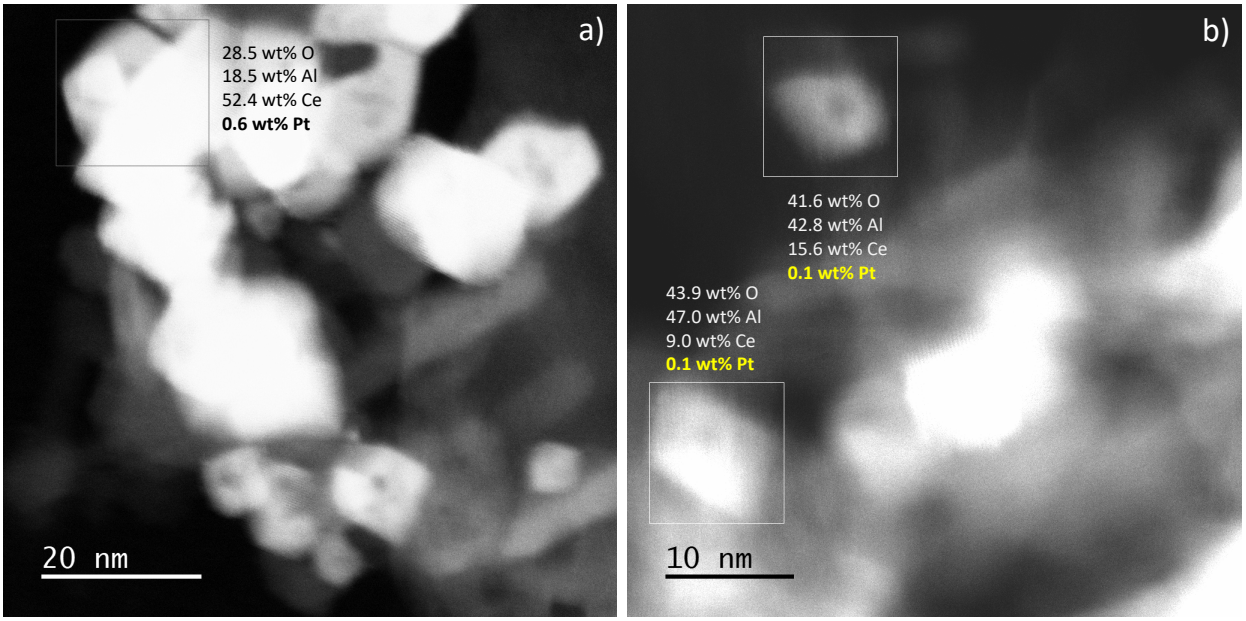

Fig. 7. AC-STEM images of the Pt_{AT}/CA08 catalyst showing EDS analysis of (a) large ceria aggregates and (b) smaller ceria crystallites. Like the other ceria/alumina samples, we see that crystalline ceria particles are able to trap Pt in atomically dispersed form, the amount of Pt is at the limit of detection in the smallest ceria crystallites.

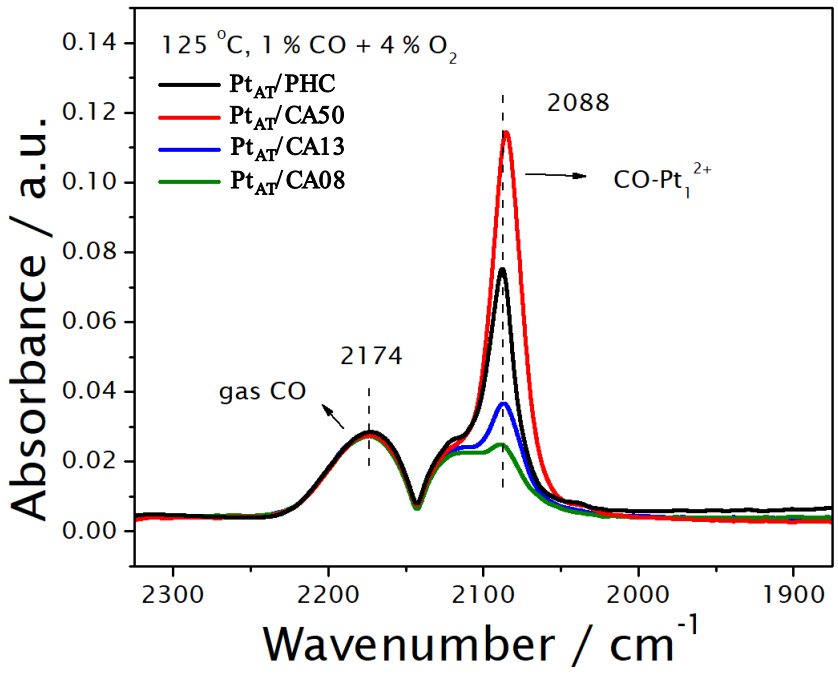

Fig. 8. CO-DRIFTS of 1 wt% Pt_{AT}/ceria-alumina and Pt_{AT}/PHC ceria catalysts. Experimental conditions: heating at 350 °C in flowing 10% O_2 for 30 min followed by pure He for 20 min; cooling in He to 125 °C, then switching to CO oxidation conditions (1% CO, 4% O_2, balance He) at 60 ml/min.

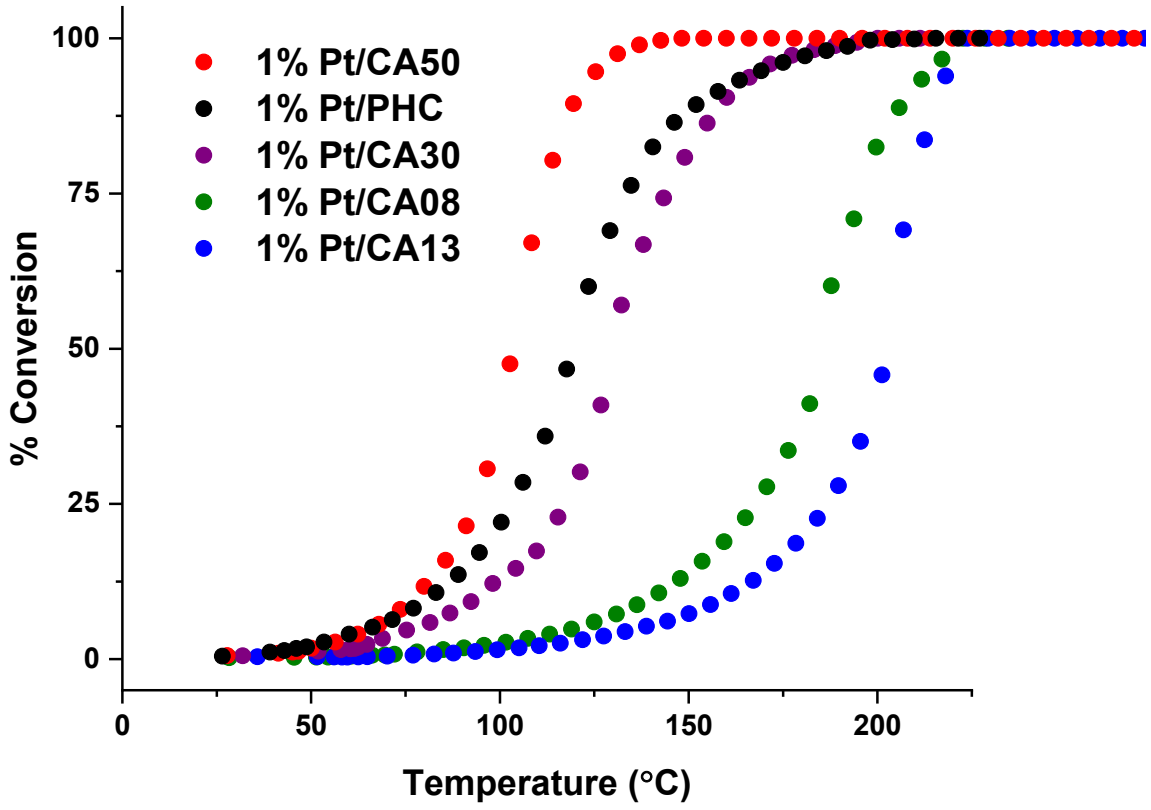

Fig. 9. CO oxidation on 1 wt% Pt_{AT}/ceria-alumina and Pt_{AT}/ceria catalysts after reduction in flowing CO. Data plotted are for the third run. Experimental conditions for CO oxidation: 20 mg sample, He = 75ml/min, CO = 1.5ml/min, O_2 = 1ml/min, ramp rate 2 °C/min to 300 °C. Reduction Treatment: He=75 ml/min and CO = 5ml/min at 275 °C for 1 hr. The improved performance of Pt_{AT}/CA50 can be attributed to smaller crystallites of ceria on the alumina, providing a higher surface area and more facile oxygen transfer to the Pt metal crystallites formed during reduction.

For Table of Contents Use Only

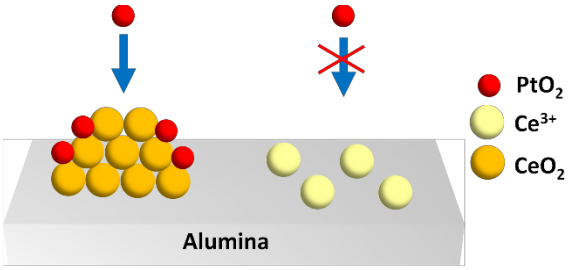

CeO_2 crystallites trap Pt in atomically dispersed form when heated at 800 °C in air. The dispersed Ce species on alumina do not trap Pt.